# Heat accumulation effects in laser processing of diamond-like nanocomposite films with bursts of femtosecond pulses

Cite as: J. Appl. Phys. **126**, 115301 (2019); https://doi.org/10.1063/1.5121424
Submitted: 24 July 2019 . Accepted: 24 August 2019 . Published Online: 16 September 2019

B. Neuenschwander, B. Jaeggi, E. V. Zavedeev, N. R. Arutyunyan, and S. M. Pimenov

Journal of Applied Physics ARTICLE scitation.org/journal/jap

# Heat accumulation effects in laser processing of diamond-like nanocomposite films with bursts of femtosecond pulses

Cite as: J. Appl. Phys. **126**, 115301 (2019); doi: 10.1063/1.5121424
Submitted: 24 July 2019 · Accepted: 24 August 2019 ·
Published Online: 16 September 2019



B. Neuenschwander,[1,a)] B. Jaeggi,[1,b)] E. V. Zavedeev,[2] N. R. Arutyunyan,[2] and S. M. Pimenov[2,a)]

## AFFILIATIONS

[1]Bern University of Applied Sciences, Institute for Applied Laser, Photonics and Surface Technologies ALPS, Burgdorf CH-3400, Switzerland
[2]Prokhorov General Physics Institute of the Russian Academy of Sciences, Moscow 119991, Russia

[a)]**Authors to whom correspondence should be addressed:** beat.neuenschwander@bfh.ch and pimenov@nsc.gpi.ru
[b)]**Present address:** Lasea Switzerland SA, CH-2502 Biel/Bienne, Switzerland.

## ABSTRACT

In this paper, we have investigated the burst mode (BM) ablation and surface structuring of diamondlike nanocomposite (DLN) a-C:H:Si:O films with femtosecond laser pulses (wavelength $\lambda = 515$ nm, pulse duration $\tau = 320$ fs, and pulse repetition rate $f = 100$ kHz) under different scanning conditions (single spots and linear structures). The pulse separation in the bursts is 25 ns (intraburst frequency $f = 40$ MHz), and the pulse number is varied from 1 to 8. The ablation depth and specific ablation rates ($\mu m^3/\mu J$) are found to be higher for the burst mode compared to single-pulse irradiation, increasing with the pulse number in the burst. The obtained experimental data of the higher ablation efficiency are shown to correlate with computer simulations of the BM ablation. In correlation with the ablation findings, Raman spectra of single spots and microgrooves have evidenced a growing graphitization of the amorphous film structure with the pulse number in the bursts (at an equal energy deposited into the films). Contact-mode atomic force microscopy (AFM) is applied to reveal an influence of the BM processing on the surface properties (nanoscale relief, friction) of laser-structured films. Based on the ablation and Raman data analysis, AFM examination of ablated/redeposited layers, and computer simulations of the burst mode ablation, the heat accumulation is identified as the main factor responsible for the enhanced ablation efficiency during the BM processing of DLN films. In addition, results of the high precision surface microstructuring of DLN films in the burst mode are presented.



## I. INTRODUCTION

Laser material processing with bursts of ultrashort (picosecond, femtosecond) pulses has been of great interest due to the possibilities of reaching higher ablation rates at lower fluences, high precision in surface microstructuring, and effects of heat accumulation on the ablation process and on the structure and surface quality of the ablated materials.[1–16] The burst mode (BM) processing of metals (steel and copper) and semiconductors (silicon) was mostly investigated. These studies showed that the resulting ablation efficiency and surface quality were strongly dependent on the pulse duration and time spacing between pulses in the burst. The analysis of the influence of bursts on the ablation process was focused around the well-established dependence of the specific removal rate vs fluence, characterized by an optimum (i.e., maximum) value for any ablated material.[4,7,16,17] It was found that during the BM ablation, an increase in the removal rate was often caused by a smaller energy of a single pulse (SP) in the burst, which was closer to the optimum value for a maximum specific ablation rate (see Ref. 4 and references therein). Generally, the burst mode resulted in lower specific removal rates than during single-pulse processing, except for a few experiments with copper[4,7] and silicon.[6] New data were recently reported on the ultrashort pulse machining of semiconductors (Si, Ge, and GaP) and dielectrics (diamondlike nanocomposite films), which showed an increased ablation efficiency in the burst mode.[18] In the case of Si, higher specific removal rates were obtained for bursts of 10-ps pulses at $\lambda = 1064$ nm, increasing by a factor of 3 for the 8-pulse

burst.[16,18] Based on calorimetric measurements on copper and also on silicon, the increased absorptivity of a rougher surface was supposed to be an effect responsible for the observed increase of the specific removal rates.[16] It was therefore concluded that the burst mode could change the surface properties in such a way that a higher ablation efficiency was achieved. In the case of diamondlike nanocomposite (DLN) a-C:H:Si:O films, preliminary data of the BM ablation under certain conditions with 2-pulse bursts evidenced the increased ablation rates compared to single pulses of the same energy, and heat accumulation was suggested to have a major effect on the ablation rates.[18,19] The heat accumulation is an attribute of ultrashort pulse material processing at high repetition rates both in the burst mode[2,4,5,8,12,13] and in the single-pulse regime,[20–22] which is generally considered as a way to achieve higher ablation rates and efficiency. At the same time, use of high average powers (high repetition rates) can significantly reduce the surface quality of the ablated material that leads to the necessity of controlling the heat accumulation in dependence on laser processing parameters.[4,20,22]

DLN films [$SiO_x$-containing hydrogenated diamondlike carbon (DLC) films][23] is a material with an amorphous structure and unique mechanical properties (high hardness, wear resistance, low friction, etc.)[24–27] required in various applications of protective and tribological coatings. DLN films are characterized by low internal stresses compared to hydrogenated DLC (a-C:H) films. This allows DLN films of a relatively large thickness (~10 $\mu$m)[25,26] to be deposited on different substrates and makes them very suitable for laser surface structuring applications. Recently, we have demonstrated that femtosecond laser surface modification and micropatterning of DLN films is an effective technique to improve and control friction properties at the microscale and macroscale.[27] Owing to very low thermal conductivity (~0.01 W/cm K) of amorphous carbon,[28] the amorphous carbon film is an interesting material for investigations of heat accumulation effects during BM ablation with femtosecond (fs) pulses. For typical values of the time spacing of 10–20 ns in the burst, the thermal diffusion length is very small (~100 nm), meaning that each next pulse in the burst interacts with the heated film surface. The "extra" heating between pulses in the burst can have a considerable influence on all the processes—graphitization, spallation, evaporation (occurring during the laser irradiation of DLC films[29–31]), and as a consequence, on the structure and surface properties of laser-processed films. It is the effects of burst mode and heat accumulation on the ablation efficiency, structure, and surface properties of DLN films which is the main goal of our research.

In this paper, we have investigated the burst mode ablation and surface micropatterning of DLN films (of 2.7 $\mu$m thickness) with fs laser pulses (wavelength $\lambda = 515$ nm, pulse duration $\tau = 320$ fs, and pulse repetition rate $f = 100$ kHz) under different scanning conditions (single spots/microcraters and linear structures/microgrooves), and the pulse number in the burst varied from 1 to 8. The specific ablation rates ($\mu m^3/\mu J$) were found to be higher for the burst mode compared to single-pulse irradiation, increasing with the pulse number in the burst (at a given pulse energy). Based on the analysis of the ablation data, structure analysis of ablated craters/grooves by Raman spectroscopy and computer simulations, the heat accumulation is identified as the main factor responsible for the enhanced ablation efficiency during the BM processing of DLN films. In addition, optimum conditions for surface microstructuring in the burst mode are specified, and highly precise surface micropatterns (microcrater/microgroove arrays) are produced on the DLN films by BM processing with fs laser pulses.

## II. EXPERIMENTAL DETAILS

The samples of DLN films on Si substrates (obtained by plasma-assisted chemical vapor deposition from a polyphenylmethyl siloxane vapor) were used in experiments of fs-laser processing in the burst mode; the deposition conditions and DLN film properties were described in detail in our previous papers.[25–27] For the samples studied, the film thickness was $h = 2.7\,\mu$m, and their hardness was $H_{IT} = 24$ GPa.

Laser surface micropatterning of the DLN samples was carried out using a SATSUMA HP2 femtosecond laser system[32,33] (from Amplitude Systèmes) generating pulses of $\tau = 320$ fs duration at the wavelength $\lambda = 515$ nm. The average power ($P$) was varied from 10 to 400 mW at the pulse repetition rate $f = 100$ kHz, corresponding to the range of pulse energy ($\varepsilon$) from 0.1 to 4 $\mu$J. The laser beam was focused with a 100-mm telecentric objective to obtain the beam radius of $w_o = 7.1\,\mu$m (related to the $1/e^2$ level). For the above pulse energies, the peak fluence, $F = 2\varepsilon/\pi p w_0^2$, was changed from $F = 0.12$ to 5 J/cm$^2$. A high precision galvanometer scanner intelli$SCAN_{se}$ from Scanlab was applied to control the scanning beam velocities ($v_s$). Two scanning regimes were used. For single spots and crater arrays (see Sec. III A), $v_s$ was from 10 m/s to 2 m/s, providing the distance between spots ($v_s/f$) of 100 $\mu$m and 20 $\mu$m, respectively. For laser processing of linear structures (microgrooves) (see Sec. III B), $v_s$ was 0.05 m/s, and the distance between adjacent spots was $v_s/f = 0.5\,\mu$m.

A scheme of the burst generation using an ultrashort pulsed laser system was reported elsewhere.[4,16] Instead of a single pulse, the pulse-picker located after the seed oscillator of the laser system was able to let pass a defined number of pulses, forming the so-called burst. The temporal spacing between the pulses in the burst was given by the oscillator frequency of about 40 MHz leading to a temporal spacing of $\Delta t_b = 25$ ns. Between the bursts, the temporal spacing was given by the used repetition rate of 100 kHz. In our ablation experiments, the pulse number ($N$) in the burst was varied from 1 to 8, and during the processing of linear groovelike structures, the pulse number was changed from 1 to 5. Three series of experiments comparing fs-laser ablation with bursts and single pulses were carried out. In the first series, single spots were produced by single pulses with increasing energy (from $\varepsilon = 0.5\,\mu$J to 4 $\mu$J) and by bursts with increasing pulse number from $N = 1$ to 8 and fixed pulse energy ($\varepsilon = 0.5\,\mu$J) so that the energy of each burst was equal to the corresponding energy of single pulse. In the second series (with single spots), the burst energy was constant ($\varepsilon_b = 0.5\,\mu$J), and the pulse number was increased from 1 to 5, leading to a proportional decrease of the pulse energy from $\varepsilon = 0.5\,\mu$J to $\varepsilon = 0.1\,\mu$J. The third series of the BM processing was related to the beam scanning experiments and groove fabrication, with a typical groove length of 15 mm and width of ~10 $\mu$m (or less, depending on the pulse energy). For correct comparison of the

ablation rates, the total laser energy per unit area was taken equal during ablation with bursts and single pulses, i.e., the depth of grooves obtained during 1 scan of $N$-pulse burst (over a given length) was compared with the depth obtained during $N$ scans (or repetitions over the same length) by single pulses. The specific removal rate is determined as the ablated volume per pulse energy ($V_{abl}/\varepsilon$) in the units of ($\mu m^3/\mu J$), which is usually obtained in experiments from the ablated volume of squares with a few millimeter side length and a few tens of micrometer depth divided by the total laser energy (equal to "average power × processing time").[4,16] In this work, the specific ablation rate (for grooves) is determined as $[S_{abl}(v_s/f)]/N\varepsilon$, where $S_{abl}$ is a cross-sectional area of a groove (relative to the original surface level) measured with an atomic force microscope, $\varepsilon$ is the pulse energy, $N$ is the pulse number in the burst or number of repetitions during single-pulse irradiation.

The surface relief of laser microcraters and micropatterns on the DLN films was examined using laser scanning microscopy (LSM), optical microscopy (OM), white-light interferometry (WLI), atomic force microscopy (AFM), and scanning electron microscopy (SEM) techniques. The structure analysis of laser-ablated film surface was performed using a Raman spectrometer LabRam (excitation wavelength: 532 nm, spectral resolution: 1 $cm^{-1}$, laser spot size: 2 $\mu$m). Raman spectra were approximated by the sum of two components: Lorenz line for the D-band and Breit–Wigner–Fano line for the G-band, as discussed elsewhere.[27] Contact-mode AFM techniques (lateral force microscopy, force-distance curves)[34] were applied to examine the surface properties of thin layers of ablated and redeposited material around the microgrooves produced with bursts and single pulses of the scanning laser beam.

## III. RESULTS AND DISCUSSION

### A. Burst mode ablation of single spots/microcraters

Initial studies of the BM ablation of single spots on the DLN film surface were focused on searching optimum conditions for producing microcraters (i) at higher ablation rates, (ii) of smaller crater size (≤10 $\mu$m diameter), and (iii) low-height protruding edges. A starting point in these experiments was done at the pulse energy $\varepsilon_{in} = 0.5\,\mu J$ (average power $P = 50$ mW) and fluence $F = 0.63$ J/cm$^2$, twice higher than the ablation threshold of $\varepsilon_{abl} = 0.25\,\mu J$ and $F_{abl} \approx 0.3$ J/cm$^2$.[27] The data comparing the ablation depth of craters obtained with bursts and single pulses are shown in Fig. 1. The surface profiles and Raman spectra of selected laser-ablated spots are displayed in Fig. 2.

As follows from Fig. 1, the ablation depth increases with a transition from single-pulse (SP) ablation, characterized by a typical logarithmic dependence of the ablation depth on pulse energy/fluence,[35–37] to the burst mode ablation for which the burst energy increases with the pulse number, i.e., $\varepsilon_b = N\varepsilon_{in}$. Estimations

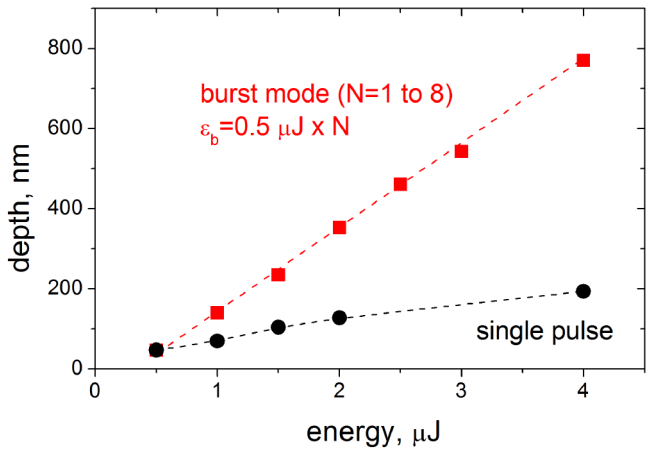


**FIG. 1.** Dependences of the ablation depth on the pulse/burst energy for single pulses and N-pulse bursts (the energy from $\varepsilon = 0.5$ to $4\,\mu J$ corresponds to the peak fluence from $F = 0.63$ to 5 J/cm$^2$).

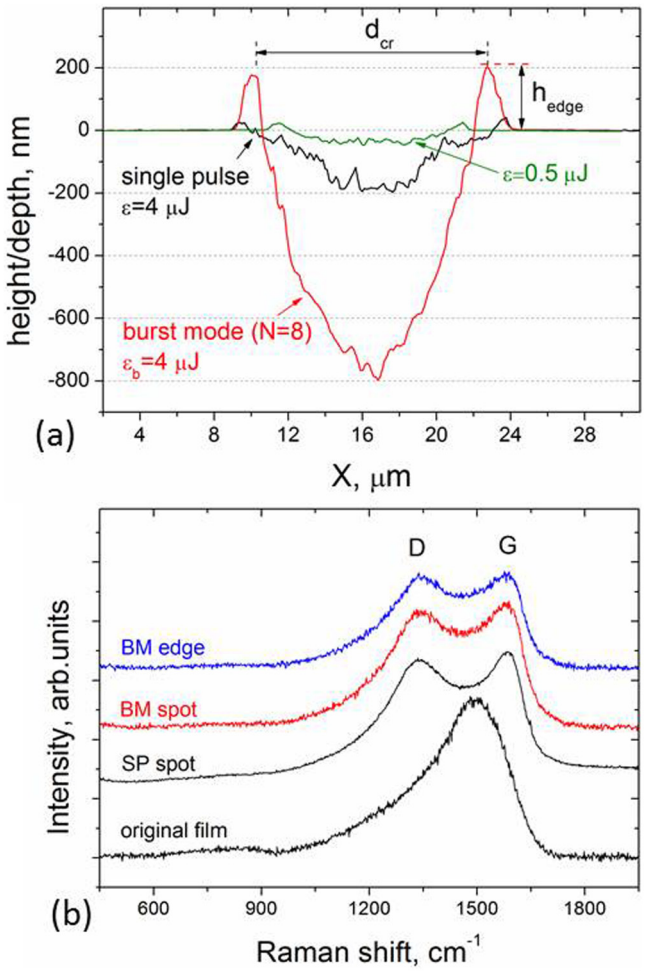


**FIG. 2.** (a) AFM surface profiles of laser spots produced by single pulses of energy $\varepsilon = 4\,\mu J$ and bursts of $N = 8$ pulses and energy $\varepsilon_b = 4\,\mu J$ (the profile produced by the single pulse of the initial energy $\varepsilon_{in} = 0.5\,\mu J$ is given for comparison) and (b) Raman spectra measured in the above spots at the center and swelling edge region (of the BM spot).

of the ablation efficiency in terms of "ablation depth per energy" show that for bursts it increases with energy, whereas for single pulses, the value ($h_{abl}/\varepsilon$) decreases with the pulse energy in accordance with the behavior of the specific removal rate[4,16,17] at fluences moving away from the optimum value. The linear dependence of the BM ablation depth on the burst energy can be qualitatively explained by a higher temperature of the film surface during irradiation with bursts. Indeed, for the time spacing of $\Delta t_b = 25$ ns, the thermal diffusion length is $(\chi \Delta t_b)^{1/2} \sim 70$ nm (where $\chi \sim 0.002$ cm$^2$/s is the thermal diffusivity of DLN films[27]) and the heat is accumulated in the very thin surface layer. The laser absorption length is $1/\alpha \sim 100$ nm or less for graphitized surface, so that each next pulse in the burst interacts with the surface layer of (much) higher temperatures (than of the original film) increased as a result of the heat accumulation from the previous pulse action ($\alpha$ is the laser absorption coefficient).

Although the enlarged ablation rates are strong, the effects of BM ablation on the crater diameter and surface quality do not satisfy the above requirements for the microstructuring of DLN films. First, the crater size increases with laser energy that is well-known for the laser processing of DLC films.[27,29] For the BM ablation, the crater diameter ($d_{cr}$) increases from $d_{cr} = 10$ to 12.6 $\mu$m, and the diameter of graphitized area ($d_{gr}$) (outer border of the spot with emerging surface swelling) increases from $d_{gr} = 11.4$ to 15.1 $\mu$m, as is seen in Fig. 2(a). Second, the swelling height of spot edges ($h_{edge}$) increases from 25 nm to ~200 nm with the pulse number ranging from $N = 1$ to 8. According to the Raman spectra in Fig. 2(b), the edge regions around craters reveal the structure of a graphitized material characterized by the appearance of two peaks—D peak at 1350 cm$^{-1}$ and G peak at 1590 cm$^{-1}$, whose parameters (position, intensity, and width) are usually used in the analysis of graphitization of amorphous carbon films.[38] The structure of the edge region is similar to that in the spot center. The graphitized surface layer is known as a softer material compared to the original DLC film,[39] so the presence of softer protruding edges of a few hundred nanometer height around microcraters is a detrimental effect for the high precision surface structuring of hard DLN coatings.

To reduce the crater size and swelling height, the BM ablation was studied at smaller pulse energies. In these experiments, the average power $P = 50$ mW and burst energy $\varepsilon_b = 0.5\,\mu$J were constant, and the pulse number was increased from $N = 1$ to 5, leading to the decrease of the pulse energy from $\varepsilon = 0.5\,\mu$J to $\varepsilon = 0.1\,\mu$J (and the peak fluence from $F = 0.63$ to 0.12 J/cm$^2$). The results of the ablation depth, crater dimensions, and Raman spectra analysis are summarized in Fig. 3. Figure 3(a) confirms the enhanced ablation efficiency for the BM irradiation of the DLN films, illustrating that the ablation depth increases from ~50 nm (for $N = 1$) to 180 nm for the 5-pulse burst. Interestingly, the energy $\varepsilon = 0.1\,\mu$J was found to be the graphitization threshold of DLN films for single-pulse irradiation,[27] and the transition from the surface graphitization (induced by the 1st pulse action) to the ablation regime occurred during irradiation with the 5-pulse bursts due to the increased light absorption in the graphitized surface layer. AFM examination of laser spots indicated that the spallation mechanism[29] might be important; however, a relative contribution of the two mechanisms (spallation and evaporation) in the enhanced ablation with bursts is not clear yet. For fs laser pulses, the thickness of spalled layers was reported to be ~10 nm, which was suggested to depend on the character of laser-induced graphitization governing the formation and propagation of high internal stresses in the film.[29]

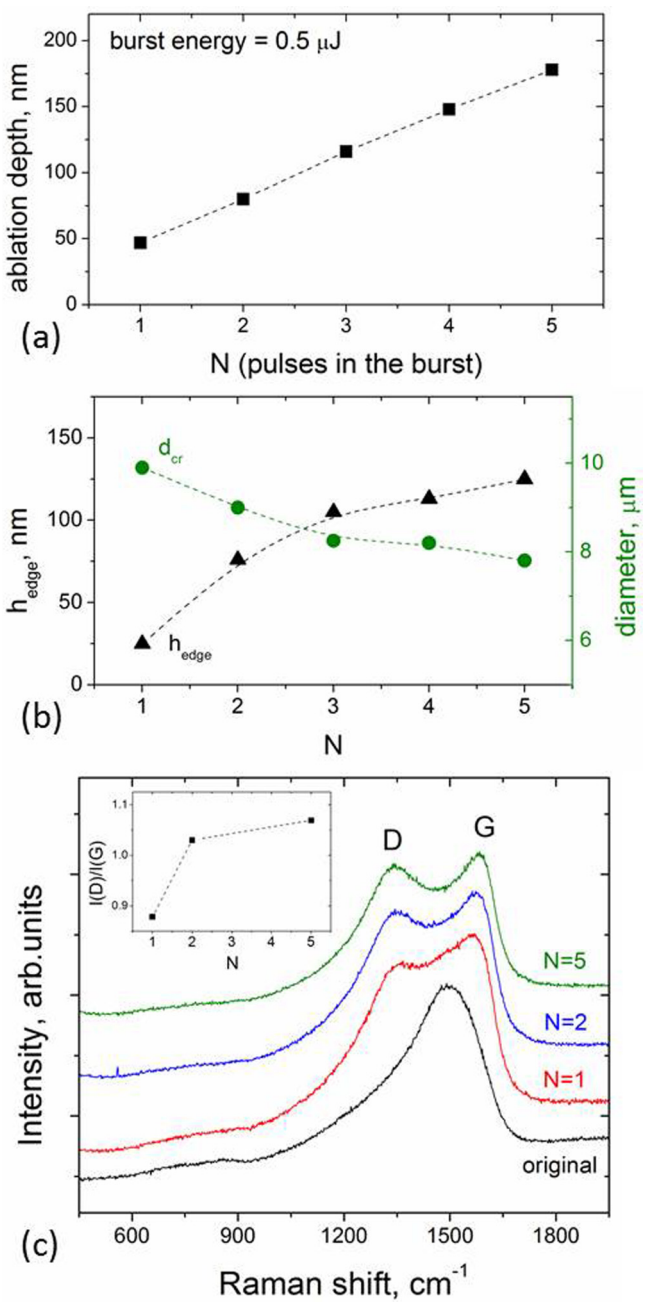


**FIG. 3.** Ablation depth (a), diameter (b), height of swelling edges (b), and Raman spectra (c) of laser spots produced at the constant burst energy $\varepsilon_b = 0.5\,\mu$J and different pulse numbers in the bursts; inset in (c) shows the ratio I(D)/I(G) vs number of pulses in the burst.

Changes in the Raman spectra of laser spots produced by BM ablation at $\varepsilon_b = 0.5\,\mu J$ evidence a growing graphitization of the amorphous structure with the pulse number [Fig. 3(c)]. The ratio of integral intensities of the D and G peaks, I(D)/I(G), usually applied for the estimation of the graphitic cluster size ($L_a$) from a relationship $I(D)/I(G) \propto L_a^2$ (for $L_a < 2$ nm in amorphous carbon),[38] can be used as a measure of "graphitization degree". Indeed, the I(D)/I(G) ratio increases with N [shown in the inset of Fig. 3(c)] as well as the graphitic cluster size $L_a$ from ~1.25 to 1.4 nm—the behavior typically observed for the laser graphitization of DLC films when the energy deposition into the films is increased.[27,39] Under the constant energy of bursts, heat accumulation between pulses appears to be a key factor of increased energy absorption and more intensive graphitization clearly pronounced in the Raman spectra.

Important information for patterning is given in Fig. 3(b) which shows that the crater size decreases and swelling height increases with the pulse number. These data were used to make a choice between two patterning regimes, depending on the pulse energy and pulse repetition rate, particularly: (i) 2-pulse burst ablation at pulse energy $\varepsilon = 0.25\,\mu J$ and low pulse repetition rates ($f = 100$ kHz) and (ii) ablation with single pulses of $\varepsilon = 0.25\,\mu J$ at high pulse repetition rates of $f = 500$ kHz to 1 MHz (in the case of linear structure fabrication). As an example, AFM images in Fig. 4 demonstrate high precision and reproducible fabrication of the microcrater array (crater diameter $d_{cr} = 9\,\mu$m and depth $h_{abl} = 2\,\mu$m) in the DLN film by 2-pulse burst ablation. Such kinds of laser-micropatterned DLN coatings were found to exhibit improved friction and wear properties under lubricated sliding.[19]

### B. Burst mode processing with scanning beam

Comparative studies of multipulse ablation with bursts and single pulses were carried out under conditions of laser beam scanning at the scanning velocity $v_s = 5$ cm/s and $f = 100$ kHz. Microgrooves were fabricated by ablation (i) with $N$-pulse bursts (at a given pulse energy varied from $\varepsilon = 0.1$ to $0.35\,\mu J$) over the fixed length and (ii) with single pulses of the same energy and $N$ repetitions of the beam scanning along the groove length. SEM image of a typical microgroove of 10-$\mu$m width and ~1.8-$\mu$m depth produced on the DLN film by multipulse ablation with a scanning beam is shown in Fig. 5. It is seen that a certain part of the ablated film material is redeposited near the groove, with micrometer-sized fragments (formed by spallation) located inside and outside the groove. In the further comparative analysis of fs-laser processing with bursts and single pulses, the ablation parameters (ablation depth, specific ablation rates), features of structural transformation (graphitization), and surface quality (swelling groove edges, redeposited material) are considered.

The data of the ablation depth and specific ablation rates of microgrooves obtained with bursts and single pulses are presented in Fig. 6. The ablation depths and ablated volumes of the grooves are compared for 1 scan of $N$-pulse bursts (marked 2p/1rep, …, 5p/1rep) and $N$ scans (or repetitions) of single pulses of the same energy (marked 1p/2rep, …, 1p/5rep). It should be emphasized that the ablation depth/specific ablation rates of the DLN films processed with bursts have proved to be higher than the ablation rates

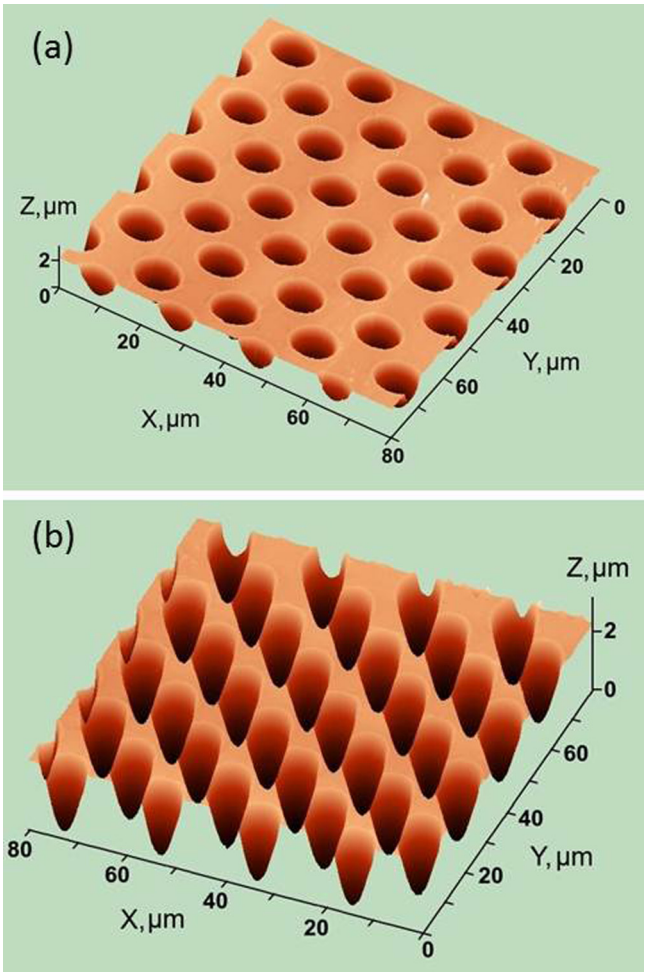


**FIG. 4.** AFM images of a microcrater array (crater diameter 9 $\mu$m, depth 2 $\mu$m, period 14 $\mu$m) produced by 2p-burst ablation: (a) top view and (b) view from inside the DLN film.

with single pulses under all the conditions studied. For the minimum energy ($\varepsilon = 0.1\,\mu J$), a huge increase from ~1 $\mu m^3/\mu J$ to 6–7 $\mu$m3/$\mu J$ was observed by applying 4-pulse and 5-pulse bursts during the beam scanning. An evident limitation of this study is concerned with the film thickness. This does not allow us to obtain the ablation characteristics over a wider range of pulse energies/fluences and to find the optimal values of the specific removal rates (used for bulk materials[4,16,17]). Particularly, processing with 3-pulse bursts at $\varepsilon = 0.25\,\mu J$ leads to the ablation of a through hole in the film. For the 4-pulse and 5-pulse bursts, the maximum pulse energy is further decreased because of the film thickness limit.

Figure 6(b) shows the results of computer modeling of specific ablation rates in comparison with the experimental data of the groove profiles. At the first step of modeling, the ablation curve for single pulses (marked as "1p burst") was obtained from the fitting with the experimental data under the variation of the laser

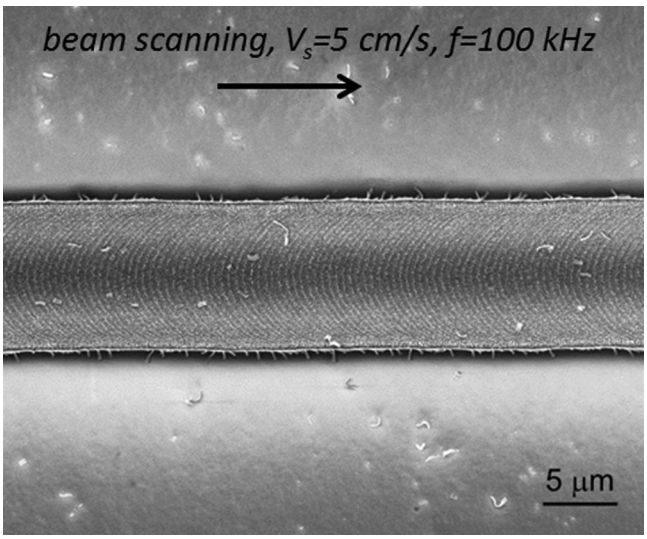


**FIG. 5.** SEM image of a typical microgroove of 10-$\mu$m width produced in the DLN film by scanning laser beam at $v_s = 5$ cm/s and $f = 100$ kHz (2-pulse burst, $\varepsilon_b = 0.5\,\mu$J).

absorption coefficient and threshold energy in accordance with the formula from Refs. 4 and 16 (expressed in terms of pulse energy),

$$\Delta V_{abl}/\Delta\varepsilon = (1/2\alpha)\cdot(\pi w_0^2/2\varepsilon)\cdot \ln^2(\varepsilon/\varepsilon_{th}), \tag{1}$$

with the absorption coefficient $\alpha = 2.5\times10^5\,\mathrm{cm}^{-1}$ and threshold energy $\varepsilon_{th} = 0.074\,\mu J$ being found to give the best fit. For the original film, the absorption coefficient is $\alpha_o = 5.6\times10^4\,\mathrm{cm}^{-1}$,[27] so the coefficient $\alpha = 2.5\times10^5\,\mathrm{cm}^{-1}$ is related to the laser absorption in the films graphitized during multipulse ablation, and this value of $\alpha$ is used in further modeling of the burst mode ablation. In the calculations, we used the beam radius ($w_o = 5.6\,\mu$m) determined from the width of ablated grooves by the Liu method[40] (it proved to be smaller than the beam radius of 7.1 $\mu$m measured with a scanning slit beam profiler). It should be noted that for the single-pulse irradiation at $f = 100$ kHz, an influence of heat accumulation between successive pulses was neglected because the heat penetration depth $(\chi/f)^{1/2} \sim 1.5\,\mu$m ($\chi \sim 0.002\,\mathrm{cm}^2/\mathrm{s}$) was comparable to the film thickness. The thermal diffusivity of the substrate is $\chi_{Si} \sim 0.8\,\mathrm{cm}^2/\mathrm{s}$ which makes it an effective cooler. Using the obtained values of $\alpha$ and $F_{th}$, numerical simulations showed that the surface temperature rise before the action of each next pulse did not exceed several tens of degrees.

In the case of the burst mode ablation, a scheme of simulations and assumptions made is briefly described below. First, the total ablated volume of a groove (of length$\gg 2w_o$), equal to the product of the groove cross section and length, is proportional to the number of spots (i.e., number of $N$-pulse bursts) multiplied by the pitch length $v_s/f = 0.5\,\mu$m. This simply means that the specific ablation rate amounts to the volume of a crater ablated during the action of one $N$-pulse burst divided by $N\varepsilon$. Second, we assume that

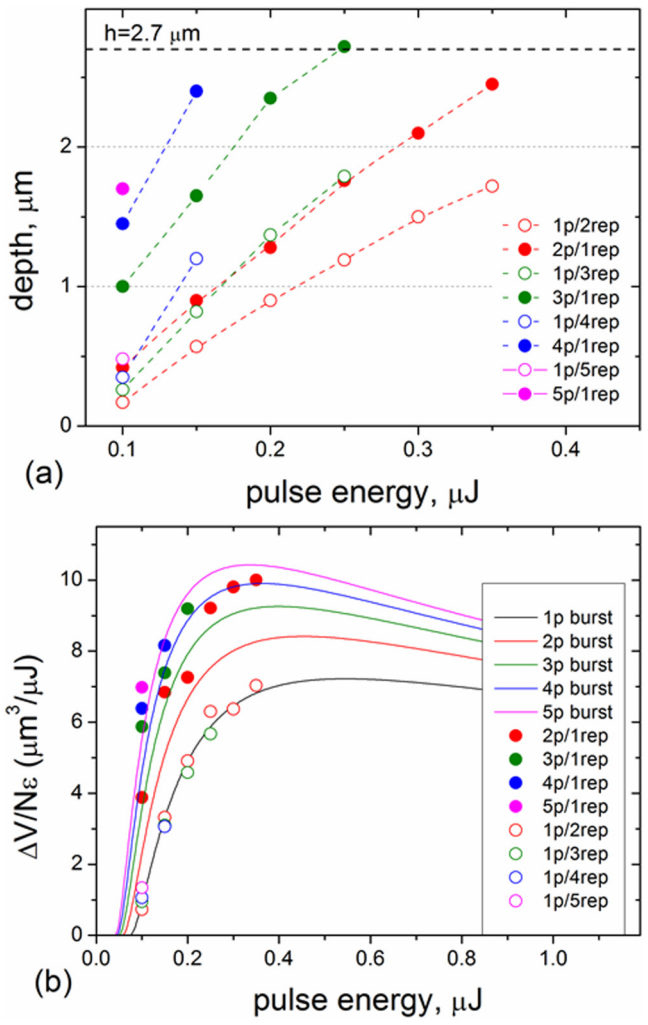


**FIG. 6.** Depth (a) and specific ablation rate (b) of microgrooves obtained under the single-pulse and burst mode irradiation conditions during laser beam scanning at $v_s = 5$ cm/s and $f = 100$ kHz [dashed line in (a) corresponds to the film thickness $h = 2.7\,\mu$m].

the material is ablated if the local fluence exceeds the threshold value $F_{th}$, light absorption is linear, and thermal conduction properties are not temperature-dependent (as is known, laser ablation of amorphous carbon films occurs without melting, and sublimation temperature is ~4000 K[31,41]).

Then, we calculate the ablation depth and ablated volume for the first and next pulses in the burst as follows:

1. The first pulse of the burst.

The ablation depth for the first pulse of the burst is given by

$$h_1(r) = \alpha^{-1}\cdot(\ln(F/F_{th}) - 2r^2/w_0^2), \tag{2}$$

where $r$ is the distance from the spot center in the radial direction [the ablation zone: $r < w_0(\ln(F/F_{th})/2)^{1/2}$].

Immediately after the absorption of the first pulse, the distribution of the accumulated energy per unit volume ($u_{acc}$) is

$$u^*_{acc,1}(r, z) = \alpha F_{acc,1}(r) \cdot \exp(-\alpha z), \quad (3)$$

where $z$ is the distance along the normal to the film surface, $F_{acc,1}(r)$ is equal to $F_{th}$ within the ablation zone and to $F\exp(-2r^2/w_0^2)$ around it.

The heat penetration depth is equal to

$$L^*_{acc,1}(r) = \pi^{1/2}/\alpha, \quad (4)$$

where the $\pi^{1/2}$ is the normalization factor related to the difference in the mean heat penetration depths for exponential and Gaussian (used below) distributions. The data ($F_{acc}$, $L^*_{acc}$) are used to determine the heat distribution at the beginning of the next pulse action.

2. The $j$th pulse of the burst.

It is assumed that the distribution of heat along the $z$ axis takes a Gaussian shape during its transfer into the film,

$$u_{acc,j}(r, z) = 2F_{acc,j-1}(r) \cdot \exp[-z^2/L_{acc,j}(r)^2]/[\pi^{1/2} \cdot L_{acc,j}(r)], \quad (5)$$

$$L_{acc,j}(r) = [L^*_{acc,j-1}(r)^2 + 4\chi\Delta t_B]^{1/2}. \quad (6)$$

After the absorption of the $j$th pulse, the heat distribution is given by

$$u_j(r, z) = u_{acc,j}(r, z) + \alpha F \cdot \exp[(-2r^2/w_0^2) - \alpha z]. \quad (7)$$

Inside the ablation zone [where $u_j(r,0) > \alpha F_{th}$], equation $u_j(r,z) = \alpha F_{th}$ was solved numerically to find the ablation depth $h_j(r)$, outside the ablation zone $h_j(r) = 0$.

The energy left in the material after ablation is

$$F_{acc,j}(r) = F'_{acc,j}(r) + F''_{acc,j}(r), \quad (8)$$

where $F'_{acc,j}(r) = F \cdot \exp[(-2r^2/w_0^2) - \alpha h_j(r)]$ is the contribution of the $j$th pulse, and $F''_{acc,j}(r) = F_{acc,j-1}(r) \cdot [1 - \mathrm{erf}(h_j(r)/L_{acc(j)}(r))]$ is the energy remained from previous pulses.

The heat penetration depth is

$$L^*_{acc,j}(r) = \{\pi^{1/2} \cdot F'_{acc,j}(r)/\alpha + [L_{acc,j}(r) \cdot \exp(-h_j^2/L_{acc,j}(r)^2)/ (1 - \mathrm{erf}(h_j(r)/L_{acc,j}(r))) - \pi^{1/2} \cdot h_j(r)] \cdot F''_{acc,j}(r)\}/F_{acc,j}(r). \quad (9)$$

The algorithm described for the $j$th pulse is repeated the required number of times. As an example, we estimate the energy accumulation during irradiation with the 5-pulse burst and pulse energy $\varepsilon = 0.1\,\mu$J. Applying the above algorithm and formulae (2)–(9), we obtain that the energy of about 0.32 $\mu$J (from total 0.4 $\mu$J of four previous pulses) is stored in the surface layer of <220 nm thickness before the action of the 5th pulse in the burst (a small energy spent for ablation is a result of the pulse energy close to the ablation threshold). Note that only 0.004 $\mu$J of single-pulses (of $\varepsilon = 0.1\,\mu$J) is spent for ablation, 5 times smaller than that with the bursts.

Finally, the ablated volume is calculated by the integral

$$V_{abl} = \sum_{j=1}^{N} \int_0^{r_{max}} 2\pi\, r h_j(r) dr, \quad (10)$$

where $r_{max}$ is the boundary of the ablation zone for the last ($N$th) pulse in the burst.

The results of numerical modeling of ablation with 2- to 5-pulse bursts [in Fig. 6(b)] clearly show the effect of the pulse number on the specific ablation rates. With increasing $N$ in the burst, the maximum specific rate is increased and shifted to lower pulse energies (fluences), which is a direct consequence of the influence of heat accumulation (between pulses in the bursts) on the BM ablation. The experimental data are in good (qualitative) correlation with the modeling; however, the obtained values of the

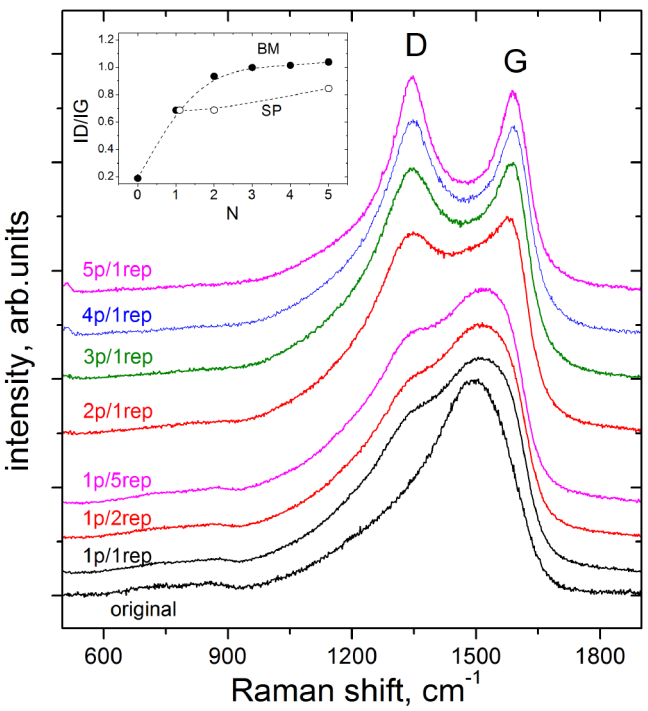


**FIG. 7.** Raman spectra measured in microgrooves fabricated by ablation with single pulses and bursts at the pulse energy $\varepsilon = 0.1\,\mu$J and variable pulse number in the burst (from 1 to 5) or number of repetitions (from 1 to 5) during laser beam scanning at $v_s = 5$ cm/s and $f = 100$ kHz; inset shows the ratio I(D)/I(G) vs N (for BM and SP irradiation).

specific ablation rates are higher than the calculated ones. The possible reasons of the observed difference between modeling and experiments are concerned with the nonlinear absorption of fs pulses, nonlinearity of heat conduction at high temperatures, contribution of the spallation mechanism (not considered in modeling) to the ablation rates, and real parameters of bursts (consisting of pulses of lowering energy) and laser beam. Further analysis of the above factors could be useful to understand a way of reducing the difference between the modeling and experimental data. In addition, the application of the proposed model to the BM ablation of other carbon materials, e.g., tetrahedral amorphous carbon film,[41] would be of interest as the spallation is missing during the laser ablation of these hydrogen-free amorphous carbon films. Nevertheless, the modeling data evidence that the BM processing conditions used in our experiments are related to the pulse energy/fluences below the optimum values providing the maximum specific removal rates. The 2-pulse burst ablation conditions are close to the optimum fluence, and this is a consequence of the limited thickness of the DLN films under study.

The Raman spectra measured in the grooves fabricated by multipulse ablation with bursts and single pulses at minimum pulse energy $\varepsilon = 0.1\,\mu J$ and variable pulse number in the burst or number of repetitions are shown in Fig. 7. Changes in the spectra of the grooves processed with bursts give a definite proof of the growing graphitization with the pulse number, especially in comparison with minor changes in the spectra of grooves ablated with single pulses. The structural transformations in the DLN film correlate with a large increase of the specific ablation rates (from $\sim 1\,\mu m^3/\mu J$ to $6–7\,\mu m^3/\mu J$) observed for the 4-pulse and 5-pulse bursts. Similar to the above discussions (of the results in Fig. 3), these findings indicate the key role of the heat accumulation in the BM processing of amorphous carbon films.

Interesting results were obtained from AFM examination of the film surface in the vicinity of the ablated grooves using the lateral (friction) force microscopy (LFM) technique. The LFM allows us to obtain the surface relief and lateral force images from the same scan[42] and to compare the nanoscale relief and friction properties of the laser-modified surface and original film.[27,34] Friction force (FF) images/profiles are obtained by the subtraction of two lateral force images/profiles recorded during tip scanning in the forward and backward directions, reducing the contribution of a surface relief slope to the lateral force signal. The FF images and surface profiles across the grooves produced by single pulses of $\varepsilon = 0.1\,\mu J$ (and 5 repeated scans) and 5-pulse bursts of $\varepsilon_b = 0.5\,\mu J$ are compared in Fig. 8; the irradiation conditions are marked as 1p/5rep and 5p/1rep, respectively. In addition to the higher ablation depth and specific ablation rate (for the 5p/1rep irradiation) discussed above, the width of the redeposit region ($w_{red}$) near the grooves is found to be larger for the BM ablation [see the surface relief profiles in Figs. 8(b) and 8(d)]. The values of $w_{red} = 20.6\,\mu m$ and $w_{red} = 42\,\mu m$ are determined for the 1p/5rep for 5p/1rep ablation conditions. This fact indicates a higher kinetic energy of ablated particles (in the course of the 5p/1rep irradiation) which is known to increase with the surface temperature during

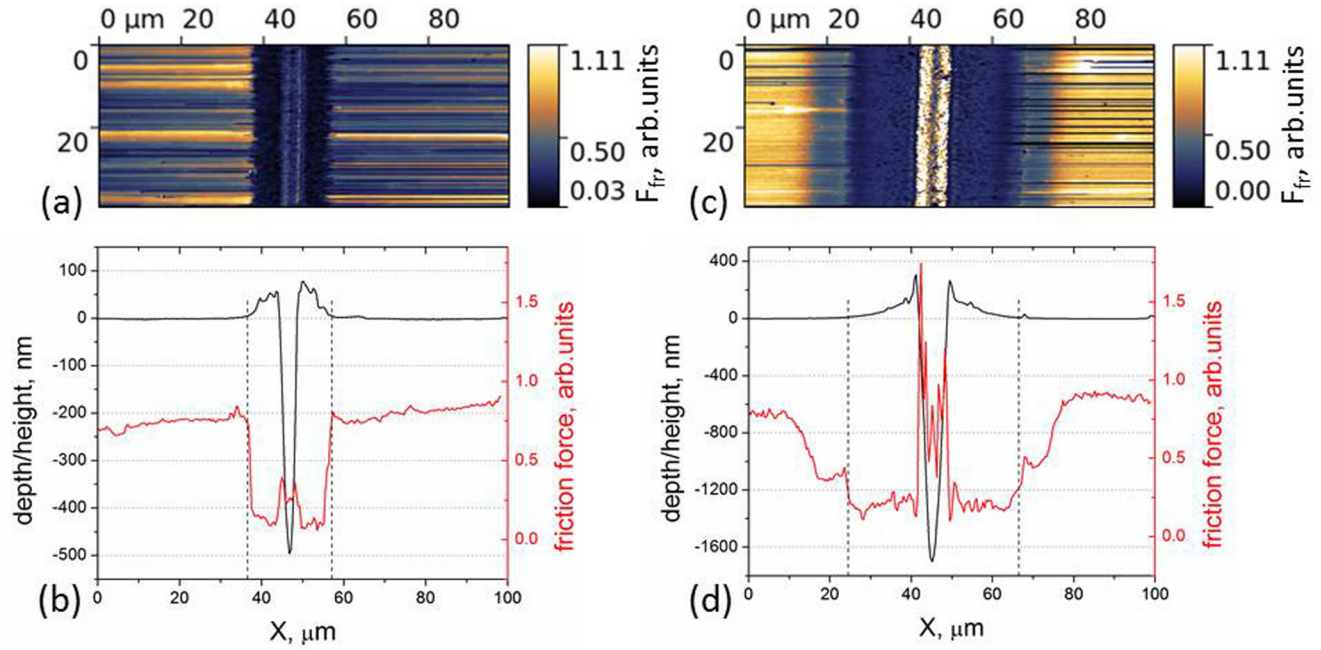


**FIG. 8.** Friction force images [(a) and (c)] and surface relief profiles with the corresponding FF profiles [(b) and (d)] across the grooves produced by single pulses and 5-pulse bursts: (a) and (b) single pulses of $\varepsilon = 0.1\,\mu J$ and 5 repeated scans of laser beam, (c) and (d) 5-pulse bursts of $\varepsilon_b = 0.5\,\mu J$ and 1 scan. LFM imaging at load F = 150 nN and RH = 65%.

evaporation,[43] thus additionally confirming the role of heat accumulation effects during the BM ablation.

Another important feature of the AFM/LFM data in Fig. 8 is that the surface regions with a thin layer of ablated and redeposited material are characterized by low-friction properties compared to the original film surface. Such a friction behavior at the nano/microscale was recently explained by (i) tip wear during LFM imaging and increased tip radius, (ii) increased nanoscale roughness of the ablated/redeposited layer, and (iii) much lower capillary force (between the worn tip and ablated surface) resulting in a much lower friction in the regions of the redeposit layer.[34] For single pulses (1p/5rep regime), the low-friction regions are clearly coincident with the redeposit layer regions [see Figs. 8(a) and 8(b)]. In the case of the 5p-burst ablation, the friction behavior in/near the microgroove is more complicated, as shown in Figs. 8(c) and 8(d). One can see higher friction along the sloped walls of the deeper groove as a result of higher surface roughness on the groove walls and higher swelling height of the edges (when the contribution of the surface relief slope to the lateral force signal was difficult to compensate). Again, the lowest friction regions are coincident with the redeposit layer regions. But in addition, 10-$\mu$m-wide regions with the friction forces higher than on the redeposit layer and lower than on the original film are observed, the origin of which (due to the formation of an ultrathin layer of more energetic nanoparticles during the ablation or the lubricating effect of graphitized nanoparticles transferred from the redeposit layer to the original surface) is not completely clear. The obtained results lead to two complementary conclusions. The ablation and surface structuring of DLN films with bursts of fs pulses is a promising approach for the fabrication and control of low-adhesive surfaces using AFM/LFM techniques with potential applications in nanotribology, micromechanical systems. On the other hand, the analysis of nanoscale friction behavior has proved, unexpectedly, to be useful to get information about the ablation dynamics during fs-laser processing of hard amorphous carbon films.

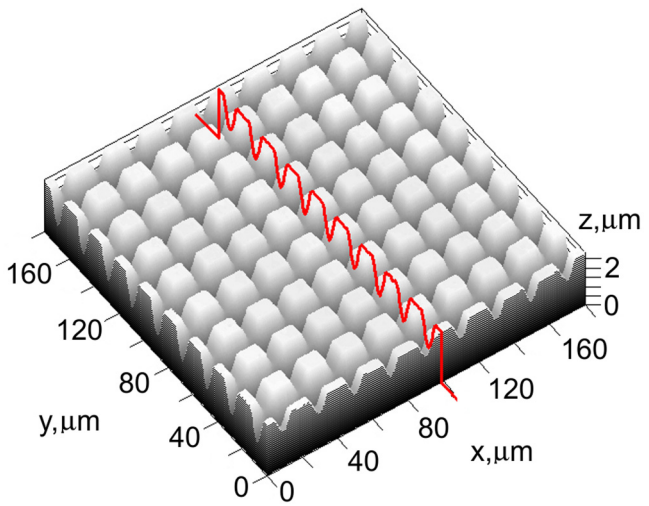


**FIG. 9.** LSM image of a crosslike microgroove pattern on the DLN sample: groove width 10 $\mu$m, period 20 $\mu$m, depth of horizontal grooves (parallel to the X axis) is 1.8 $\mu$m and depth of vertical grooves is 0.9 $\mu$m.

Similar to the processing of microcrater arrays, i.e., because of growing graphitization of the DLN films and increasing height of the groove edges with the pulse number in the burst, we used the regime of 2-pulse burst ablation at $\varepsilon = 0.25\,\mu$J, $f = 100$ kHz, and $v_s = 5$ cm/s for the fabrication of microgroove patterns. Changing the beam scanning direction by 90° after the fabrication of a parallel microgroove pattern in one direction enables us to produce a crosslike pattern, shown in Fig. 9. The crosslike pattern was produced on the film surface area of $6 \times 10$ mm$^2$ (processing time 154 s) and was characterized by the groove width of 10 $\mu$m, depth of horizontal grooves of 1.8 $\mu$m and vertical grooves of 0.9 $\mu$m, and period of 20 $\mu$m. The applied regime of 2-pulse burst ablation provides fast and high precision processing of the DLN films.

## IV. CONCLUSIONS

Laser processing of hard amorphous carbon coatings with bursts of femtosecond pulses has proved to be an interesting technique to reveal the influence of heat accumulation on the enhanced ablation rates and transformations in the structure and properties of the films. First, the specific ablation rates of the DLN films processed with bursts were found to be higher than those with single pulses under all the ablation regimes studied. These findings correlate with computer simulations which are based exclusively on considerations of heat accumulation effects during the BM ablation process. Second, Raman spectra analysis of the grooves processed with bursts provided a convincing proof of the growing graphitization with the pulse number as compared with minor changes in the spectra of grooves ablated with single pulses. The structural transformations correlate with a large increase of the specific ablation rates and confirm the key role of the heat accumulation in the BM processing of the DLN films. Third, AFM/LFM surface analysis showed a larger width of a thin redeposited layer (coinciding with the width of low-friction regions in LFM images) near the grooves processed with bursts, resulting from a higher kinetic energy of the ablated particles due to higher surface temperatures achieved by heat accumulation between pulses in the bursts. Based on the ablation and film property investigations, optimum conditions for surface microstructuring in the burst mode are specified, and highly precise microcrater/microgroove patterns have been fabricated on the DLN films by the BM processing with fs laser pulses.

## ACKNOWLEDGMENTS

The authors thank Dr. Mikhail Shupegin for chemical vapor deposition of DLN films and Josef Zuercher for the help with SEM images. This work was supported by the Russian Science Foundation under Project No. 15-12-00039.

## REFERENCES

[1]R. Knappe, H. Haloui, A. Seifert, A. Weis, and A. Nebel, Proc. SPIE **7585**, 75850H (2010).
[2]W. Hu, Y. C. Shin, and G. King, Appl. Phys. A **98**, 407–415 (2010).
[3]F. Zimmermann, S. Richter, S. Döring, A. Tünnermann, and S. Nolte, Appl. Opt. **52**, 1149–1154 (2013).

[4]B. Neuenschwander, T. Kramer, B. Lauer, and B. Jaeggi, Proc. SPIE **9350**, 93500U (2015).
[5]C. Kerse, H. Kalaycıoğlu, P. Elahi, B. Çetin, D. K. Kesim, Ö. Akçaalan, S. Yavaş, M. D. Aşık, B. Öktem, H. Hoogland, R. Holzwarth, and F. Ö. Ilday, Nature **537**, 84–88 (2016).
[6]C. Gaudiuso, H. Kämmer, F. Dreisow, A. Ancona, A. Tünnermann, and S. Nolte, Proc. SPIE **9740**, 974017 (2016).
[7]T. Kramer, Y. Zhang, S. Remund, B. Jaeggi, A. Michalowski, L. Grad, and B. Neuenschwander, J. Laser Micro/Nanoeng. **12**, 107–114 (2017).
[8]J. Mur, J. Petelin, N. Osterman, and R. Petkovšek, J. Phys. D Appl. Phys. **50**, 325104 (2017).
[9]J. Mur, L. Pirker, N. Osterman, and R. Petkovšek, Opt. Express **25**, 26356–26364 (2017).
[10]M. E. Povarnitsyn, P. R. Levashov, and D. V. Knyazev, Appl. Phys. Lett. **112**, 051603 (2018).
[11]D. J. Förster, S. Faas, S. Gröninger, F. Bauer, A. Michalowski, R. Weber, and T. Graf, Appl. Surf. Sci. **440**, 926–931 (2018).
[12]B. Jäggi, D. J. Förster, R. Weber, and B. Neuenschwander, Adv. Opt. Technol. **7**, 175–182 (2018).
[13]C. Gaudiuso, G. Giannuzzi, A. Volpe, P. M. Lugarà, I. Choquet, and A. Ancona, Opt. Express **26**, 3801–3812 (2018).
[14]G. Giannuzzi, C. Gaudiuso, C. Di Franco, G. Scamarcio, P. M. Lugaràa, and A. Ancona, Opt. Lasers Eng. **114**, 15–21 (2019).
[15]J. Mur and R. Petkovšek, Appl. Surf. Sci. **478**, 355–360 (2019).
[16]B. Neuenschwander, B. Jaeggi, D. J. Foerster, T. Kramer, and S. Remund, J. Laser Appl. **31**, 022203 (2019).
[17]G. Račiukaitis, M. Brikas, P. Gečys, B. Voisiat, and M. Gedvilas, J. Laser Micro/Nanoeng. **4**, 186–191 (2009).
[18]B. Neuenschwander, B. Jaeggi, S. M. Remund, and S. M. Pimenov, Proc. SPIE **10519**, 1051904 (2018).
[19]S. M. Pimenov, B. Jaeggi, B. Neuenschwander, E. V. Zavedeev, O. S. Zilova, and M. L. Shupegin, Diam. Relat. Mater. **93**, 42–49 (2019).
[20]F. Bauer, A. Michalowski, T. Kiedrowski, and S. Nolte, Opt. Express **23**, 1035–1043 (2015).
[21]T. V. Kononenko, C. Freitag, M. S. Komlenok, V. Onuseit, R. Weber, T. Graf, and V. I. Konov, J. Appl. Phys. **118**, 103105 (2015).
[22]R. Weber, T. Graf, C. Freitag, A. Feuer, T. Kononenko, and V. I. Konov, Opt. Express **25**, 3966–3979 (2017).
[23]V. F. Dorfman, Thin Solid Films **212**, 267–273 (1992).
[24]T. W. Scharf, J. A. Ohlhausen, D. R. Tallant, and S. V. Prasad, J. Appl. Phys. **101**, 063521 (2007).
[25]E. V. Zavedeev, O. S. Zilova, M. L. Shupegin, A. D. Barinov, N. R. Arutyunyan, T. Roch, and S. M. Pimenov, Appl. Phys. A **122**, 961 (2016).
[26]E. V. Zavedeev, O. S. Zilova, A. D. Barinov, M. L. Shupegin, N. R. Arutyunyan, B. Jaeggi, B. Neuenschwander, and S. M. Pimenov, Diam. Relat. Mater. **74**, 45–52 (2017).
[27]S. M. Pimenov, E. V. Zavedeev, N. R. Arutyunyan, O. S. Zilova, M. L. Shupegin, B. Jaeggi, and B. Neuenschwander, J. Appl. Phys. **122**, 145301 (2017).
[28]A. A. Balandin, Nat. Mater. **10**, 569–581 (2011).
[29]T. V. Kononenko, S. M. Pimenov, V. V. Kononenko, E. V. Zavedeev, V. I. Konov, G. Dumitru, and V. Romano, Appl. Phys. A **79**, 543–549 (2004).
[30]G. Dumitru, V. Romano, H. P. Weber, S. Pimenov, T. Kononenko, M. Sentis, J. Hermann, and S. Bruneau, Appl. Surf. Sci. **222**, 226–233 (2004).
[31]T. V. Kononenko, V. V. Kononenko, S. M. Pimenov, E. V. Zavedeev, V. I. Konov, V. Romano, and G. Dumitru, Diam. Relat. Mater. **14**, 1368–1376 (2005).
[32]B. Neuenschwander, B. Jaeggi, M. Schmid, and G. Hennig, Phys. Proc. **56**, 1047–1058 (2014).
[33]B. Jaeggi, B. Neuenschwander, S. Remund, and T. Kramer, Proc. SPIE **10091**, 100910J (2017).
[34]E. V. Zavedeev, B. Jaeggi, J. Zuercher, B. Neuenschwander, O. S. Zilova, M. L. Shupegin, M. Yu. Presniakov, and S. M. Pimenov, Wear **416–417**, 1–5 (2018).
[35]B. N. Chichkov, C. Momma, S. Nolte, F. vonAlvensleben, and A. Tunnermann, Appl. Phys. A **63**, 109–115 (1996).
[36]J. Krüger and W. Kautek, Appl. Surf. Sci. **106**, 383–389 (1996).
[37]P. Balling and J. Schou, Rep. Prog. Phys. **76**, 036502 (2013).
[38]A. C. Ferrari and J. Robertson, Phys. Rev. B **61**, 14095 (2000).
[39]M. S. Komlenok, N. R. Arutyunyan, V. V. Kononenko, E. V. Zavedeev, V. D. Frolov, A. A. Chouprik, A. S. Baturin, H.-J. Scheibe, and S. M. Pimenov, Diam. Relat. Mater. **65**, 69–74 (2016).
[40]J. M. Liu, Opt. Lett. **7**, 196–198 (1982).
[41]T. Roch, D. Benke, S. Milles, A. Roch, T. Kunze, and A. Lasagni, Diam. Relat. Mater. **55**, 16–21 (2015).
[42]G. Meyer and N. M. Amer, Appl. Phys. Lett. **57**, 2089–2091 (1990).
[43]A. A. Morozov, A. B. Evtushenko, and A. V. Bulgakov, Appl. Phys. Lett. **106**, 054107 (2015).